PHYSICAL REVIEW B VOLUME 49, NUMBER 5 1 FEBRUARY 1994-I

# Polymorphic phase transition for inverse-power-potential crystals keeping the first-order anharmonic correction to the free energy

Daniel H. E. Dubin
*Department of Physics, University of California at San Diego, La Jolla, California 92093-0319*

Hugh Dewitt
*Lawrence Livermore National Laboratory, P.O. Box 808, Livermore, California 94550*
(Received 9 July 1993; revised manuscript received 24 September 1993)

An improved phase diagram for the polymorphic fcc-bcc phase transition of inverse-power-potential crystals is obtained through an exact analytic calculation of the crystalline free energy including the first-order [$O(T^2)$, where $T$ is the temperature] anharmonic term in the internal energy. The anharmonic correction reduces the region of bcc stability relative to the harmonic result, in qualitative agreement with recent Monte Carlo results for the $1/r^6$ potential.

Many simple metals display a polymorphic transition from a close-packed solid to a body-centered-cubic (bcc) solid.[1] A theoretical model which exhibits this behavior is the system of particles interacting via an inverse-power potential,

$$\phi(r)=\varepsilon(\sigma/r)^n , \tag{1}$$

where for $n \le 3$ a uniform neutralizing background is also added in order to balance the collective long-range repulsive force. This model has been used to explain a possible bcc phase of iron in the center of the earth.[2]

An important simplifying feature of this family of potentials is that the classical excess free energy (the Helmholtz free energy relative to that of an ideal gas) is, when divided by $NkT$, a function only of a single scaled density parameter $\gamma_n$:

$$\gamma_n=n_0\sigma^3\left[\frac{\varepsilon}{kT}\right]^{3/n} ,$$

where $T$ is the temperature and $n_0$ is the density. Hence, the classical phase diagram can be collapsed to one dimension, with phase boundaries determined by the particular values of $\gamma_n$ at which the free energies of different phases cross. For $n=1$, Eq. (1) is the long-range Coulomb potential of a one-component plasma, while for larger values of $n$, the potential becomes shorter range, approaching that of hard spheres. The inverse powers thus conveniently offer a wide spectrum of monotonic repulsive potentials with which to study the theoretical systematics of solid phase diagrams.

Hoover, Young, and Grover[3] showed that for $n=4$ and 6, an fcc-bcc transition can occur in this system. For these $n$ values they argued that while the minimum energy state is face-centered-cubic, the looser packing of the bcc solid makes the entropy of this phase higher and hence at finite temperature, the bcc phase is favored. For $n \gtrsim 7.66$, the bcc phase becomes linearly unstable to an infinite wavelength shear mode between the (1, 1, 0) planes of the lattice.[2] The polarization of the unstable shear mode is in the (1, −1, 0) direction. Furthermore, for $n \lesssim 1.51$, the bcc crystal has lower Madelung energy, so the polymorphic transition is limited to some range of $n$ between these two values.

However, the original argument in Ref. 3 employed harmonic lattice theory, in which the free energy of the bcc and fcc crystal phases is approximated by that of a harmonic lattice. While this is a useful first approximation, according to this method the $\gamma_n$ values for which the fcc-bcc phase transition occurs lie uncomfortably close to the fcc melting transition determined by Monte Carlo simulation in Ref. 4, and so a theory based on the harmonic lattice approximation is quantitatively suspect. Indeed, recent molecular-dynamics simulations[5] for the case $n=6$ have found that the region of the stable bcc phase is considerably smaller than predicted by harmonic lattice theory. The authors conjectured that anharmonic terms in the free energy reduce the stability of the bcc phase relative to that of the fcc phase.

In this paper we present the results of a first-principles evaluation of the lowest-order anharmonic correction to the free energy for fcc and bcc crystals for $1 \le n \le 12$. We find that the anharmonic term reduces the thermodynamic stability of the bcc phase relative to the fcc phase, in qualitative agreement with the simulation results[5] for $n=6$.

Anharmonic terms in the excess Helmholtz free energy $F_e$ arise mathematically through an expansion of $F_e$ in the temperature:[6,7]

$$\frac{F_e}{NkT}(\Gamma_n)=\frac{M}{2}\Gamma_n+\frac{3}{2}\ln\left[2\left[\frac{3}{4\pi}\right]^{n/3}\Gamma_n\right]+1-S_H -\frac{A_1}{\Gamma_n}-\frac{A_2}{2\Gamma_n^2}-\frac{A_3}{3\Gamma_n^3}-\cdots , \tag{2}$$

where $\Gamma_n$ is the scaled inverse temperature (also referred to as the correlation parameter):

$$\Gamma_n\equiv\frac{\varepsilon\sigma^n}{a^n kT}=\left[\frac{4\pi}{3}\gamma_n\right]^{n/3} , \tag{3}$$

0163-1829/94/49(5)/3043(6)/$06.00  

and where $a$ is the Wigner-Seitz radius given by $4\pi n_0 a^3/3=1$. The first term in Eq. (2) is the potential energy of the lattice; $M$ is the Madelung constant. The next three terms represent the contribution of the phonon ideal gas to the excess free energy. The entropy constant $S_H$ contributes to the excess harmonic entropy, and is determined by the $3N-3$ nonzero harmonic lattice frequencies $\omega_i$:

$$S_H=\frac{1}{N}\sum_{i=1}^{3N-3}\ln\left[\frac{\omega_p}{\omega_i}\right], \tag{4}$$

where $\omega_p=\sqrt{4\pi\varepsilon\sigma^n n_0^{(n+2)/3}/m}$ is a frequency scale associated with the phonons, and $m$ is the mass of the particles. The factor of $4\pi$ is added in order that $\omega_p$ equal the plasma frequency when $n=1$.

The terms in Eq. (2) involving the $A_n$'s are anharmonic corrections to the free energy due to phonon-phonon interactions. Like Eq. (4), they can be represented by (successively more complicated) sums involving the harmonic lattice frequencies as well as the interaction potential. By performing these lattice sums using powerful Ewald sum techniques, the first-order anharmonic term $A_1$ was recently calculated for the bcc[7,8] and fcc[7] lattices in a one-component plasma ($n=1$). Here we present the results of the same calculation for other values of $n$, the only difference being that we replace the Coulomb Ewald sum $S(\mathbf{f},\mathbf{x})$ of Eq. (C2) in Ref. 7 by the inverse-power-potential generalization:

$$\begin{aligned}S_n(\mathbf{f},\mathbf{x})=\sum_{\mathbf{p}}{}'\phi(|\mathbf{p}+\mathbf{x}|)e^{i\mathbf{f}\cdot\mathbf{p}}=\frac{\varepsilon\sigma^n}{\Gamma(n/2)}\Bigg[&\sum_{\mathbf{p}}\frac{\Gamma(n/2,(|\mathbf{p}+\mathbf{x}|^2)/4R^2)}{|\mathbf{p}+\mathbf{x}|^n}e^{i\mathbf{f}\cdot\mathbf{p}},\\&-\frac{2}{3-n}\frac{\pi^{3/2}n_0}{2^{n-3}}R^{3-n}\Delta(\mathbf{f})\\&+\frac{\pi^{3/2}n_0}{2^{n-3}}\sum_{\mathbf{k}}{}'k^{n-3}\Delta(\mathbf{k}+\mathbf{f})\Gamma((3-n)/2,k^2R^2)e^{i\mathbf{k}\cdot\mathbf{x}}\Bigg]-\phi(x),\end{aligned} \tag{5}$$

where the prime on the sums indicate that the $\mathbf{p}=0$ and $\mathbf{k}=0$ terms are excluded, $\mathbf{p}$ and $\mathbf{g}$ are lattice and inverse lattice vectors, respectively, $\Delta(\mathbf{f})=\sum_{\mathbf{g}}\delta_{\mathbf{f}-\mathbf{g}}$ where $\delta$ is the Kronecker delta function, and $\Gamma(n)$, $\Gamma(n,x)$, and $\gamma(n,x)$ are gamma functions.

We evaluate $A_1$ using the exact expression obtained from perturbation theory:

$$A_1=\Gamma_n\left[\frac{\langle U_3^2\rangle}{72N(kT)^2}+\frac{\langle U_4\rangle}{24NkT}\right].$$

Here $U_n=\sum_{i,j,\ldots}\nabla_i\nabla_j\cdots\Phi\cdot\mathbf{u}_i\mathbf{u}_j\cdots$, where the $\nabla$ and $\mathbf{u}$ terms are repeated $n$ times each, $\Phi$ is the $N$-particle interaction potential evaluated at the equilibrium lattice positions, $\mathbf{u}_i$ is the displacement from equilibrium of the $i$th particle, and the average $\langle\ \rangle$ is over a distribution of displacements given by an ideal gas of phonons at temperature $T$. These averages can be written exactly in terms of sums over the phonon spectrum. For example,

$$\frac{\langle U_4\rangle}{NkT}=\frac{3kT}{m^2N^2}\sum_{\substack{\mathbf{f}_1\mathbf{f}_2\\ s_1s_2}}\frac{\mathbf{C}(\mathbf{f}_1,\ \mathbf{f}_2)\cdot\mathbf{v}(\mathbf{f}_1,\ s_1)\mathbf{v}(-\mathbf{f}_1,\ s_1)\mathbf{v}(\mathbf{f}_2,\ s_2)\mathbf{v}(-\mathbf{f}_2,\ s_2)}{[\omega(\mathbf{f}_1,\ s_1)\omega(\mathbf{f}_2,\ s_2)]^2},$$

where $(\mathbf{f}_1,\ s_1)$ denotes the wave vector and polarization index ($s=1$, 2, or 3) for a given phonon, $\mathbf{v}(\mathbf{f}_1,\ s_1)$ is the polarization unit vector, $\omega(\mathbf{f}_1,\ s_1)$ is the phonon frequency, the sums run over the first Brillouin zone, and $\mathbf{C}$ is a fourth-rank symmetric tensor defined by

$$\mathbf{C}(\mathbf{f}_1,\ \mathbf{f}_2)=2\{\chi(0)-\chi(\mathbf{f}_1)-\chi(\mathbf{f}_2)+\tfrac{1}{2}[\chi(\mathbf{f}_1+\mathbf{f}_2)+\chi(\mathbf{f}_1-\mathbf{f}_2)]\},$$

where $\chi(\mathbf{f})=\partial/\partial\mathbf{x}\,\partial/\partial\mathbf{x}\,\partial/\partial\mathbf{x}\,\partial/\partial\mathbf{x}\,S(\mathbf{f},\mathbf{x})|_{\mathbf{x}=0}$. A similar expression exists for $\langle U_3^2\rangle$:

$$\frac{\langle U_3^2\rangle}{N(kT)^2}=\frac{6kT}{m^3N^2}\sum_{\substack{\mathbf{f}_1\mathbf{f}_2\mathbf{f}_3\\ s_1s_2s_3}}\frac{|\mathbf{B}(\mathbf{f}_1,\ \mathbf{f}_2,\ \mathbf{f}_3)\cdot\mathbf{v}(\mathbf{f}_1,\ s_1)\mathbf{v}(\mathbf{f}_2,\ s_2)\mathbf{v}(\mathbf{f}_3,\ s_3)|^2}{[\omega(\mathbf{f}_1,\ s_1)\omega(\mathbf{f}_2,\ s_2)\omega(\mathbf{f}_3,\ s_3)]^2},$$

where $\mathbf{B}$ is a third-rank symmetric tensor given by

$$\mathbf{B}=[\beta(\mathbf{f}_1)+\beta(\mathbf{f}_2)+\beta(\mathbf{f}_3)]\Delta(\mathbf{f}_1+\mathbf{f}_2+f_3),$$

and $\beta(\mathbf{f})=\partial/\partial\mathbf{x}\,\partial/\partial\mathbf{x}\,\partial/\partial\mathbf{x}\,S(\mathbf{f},\mathbf{x})|_{\mathbf{x}=0}$. The double sums over the first Brillouin zone are evaluated numerically using an efficient third-order midpoint rule technique described in Ref. 7, which involves storing the values of $\mathbf{v}(\mathbf{f},\ s)$, $\omega(\mathbf{f},\ s)$, $\chi(\mathbf{f})$, and $\beta(\mathbf{f})$ on a $P\times P\times P$ lattice within the Brillouin zone, chosen so that any two vectors $\mathbf{f}$ in the lattice add to another vector on the lattice, after suitable translation by an inverse lattice vector. The double sums over the Brillouin zone are then replaced by sums over this lattice, which converge to the proper result as $P \rightarrow \infty$. This technique requires only a single evaluation of the Ewald sums at each lattice point, which greatly enhances the efficiency of the computation, allowing us to take relatively large values of $P$. Errors in the sums are determined by using increasing values of $P$ and observing the convergence. Values of $P$ up to 25 were employed in order to obtain results accurate to the number of significant figures given in Table I. Generally, we found that sums over the fcc lattice converged more rapidly than those over the bcc lattice, and bcc convergence grew worse as $n \rightarrow 7$. More details concerning the convergence properties of this technique are given in Ref. 7 for the case of $n=1$.

The results for $A_1$ as a function of $n$ are listed in Table I for both the fcc and bcc lattices, together with data for the Madelung energies $M$ and entropy constants $S_H$. These three functions of $n$ are also plotted in Figs. 1–3. Our values for $S_H$ agree well with those of Ref. 3 for $n=4$ and $n=6$ when differences in frequency conventions are properly accounted for. [Equation (4) is defined in terms of angular frequencies and normalizes to the generalized plasma frequency $\omega_p$, whereas Ref. 3 uses frequencies in $\sec^{-1}$ and employs the Einstein frequency $\nu_E$]. The Madelung energy is undefined as $n \rightarrow 3$ due to the effect of interactions between particles separated by large distances. A uniform neutralizing background

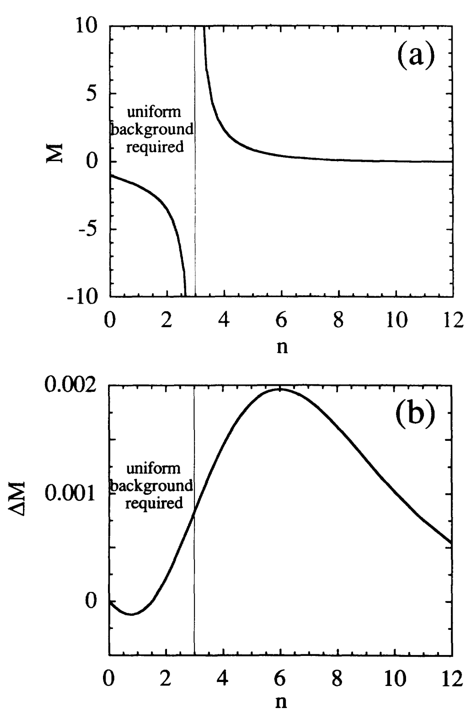


FIG. 1. (a) Madelung constants $M_{bcc}$ and $M_{fcc}$ for bcc and fcc lattices, respectively, vs $n$ for $1/r^n$ potentials. The constants were evaluated at values of $n$ given by $n=0.2m$, with $m$ a positive integer, and the curves shown are interpolations. The curves for $M_{bcc}$ and $M_{fcc}$ fall atop one another, the difference being invisible on this scale. (b) The difference $\Delta M = M_{bcc} - M_{fcc}$ vs $n$.

TABLE I. Dependence on $n$ of lattice sums appearing in the excess free energy [Eq. (2)] and the Lindemann criterion [Eq. (12)], for fcc and bcc lattices. Also shown are both the anharmonic and harmonic $\Gamma_n$ values for the fcc-bcc transition [Eqs. (7) and (8), respectively], as well as the volume and entropy changes at this transition.

| $n$ | $M_{bcc}$ | $M_{fcc}$ | $\Delta M(\times 10^{-3})$ | $S_{Hbcc}$ | $S_{Hfcc}$ | $A_{1bcc}$ | $A_{1fcc}$ | $\Gamma_{fcc-bcc}$ | $\Gamma^{Harm.}_{fcc-bcc}$ | $\Delta V/V$ | $\Delta S/Nk$ | $\langle \omega_p^2/\omega^2 \rangle_{bcc}$ | $\langle \omega_p^2/\omega^2 \rangle_{fcc}$ |
|---|---|---|---|---|---|---|---|---|---|---|---|---|---|
| 1 | −1.791 859 | −1.791 747 | −0.111 | 2.4939 | 2.4537 | 10.84 | 12.35 | | | | | 12.9 | 12.1 |
| 2 | −3.491 916 | −3.492 132 | −0.217 | 0.9674 | 0.9086 | 4.75 | 5.99 | 520 | 543 | 0 | 0.0540 | 4.43 | 3.90 |
| 3 | Undefined | Undefined | 0.833 | 0.0257 | −0.0521 | 2.65 | 4.09 | 166 | 182 | 0 | 0.0604 | 2.31 | 1.91 |
| 4 | 2.365 400 | 2.363 956 | 1.444 | −0.6403 | −0.7370 | 1.03 | 3.04 | 108 | 133 | $1.98\times10^{-4}$ | 0.0601 | 1.49 | 1.14 |
| 5 | 0.876 714 8 | 0.874 874 3 | 1.840 | −1.1395 | −1.2547 | −1.24 | 2.00 | 82.4 | 125 | $3.71\times10^{-4}$ | 0.0379 | 1.10 | 0.78 |
| 6 | 0.413 852 0 | 0.411 887 3 | 1.965 | −1.5250 | −1.6585 | −5.70 | 0.416 | | 136 | | | 0.91 | 0.57 |
| 7 | 0.212 261 5 | 0.210 399 6 | 1.862 | −1.8264 | −1.9789 | −17.8 | −2.49 | | 164 | | | 0.85 | 0.45 |
| 8 | 0.113 048 2 | 0.111 429 3 | 1.619 | | −2.2357 | | −8.00 | | | | | | 0.37 |
| 9 | 0.061 413 8 | 0.060 095 3 | 1.319 | | −2.4424 | | −18.5 | | | | | | 0.32 |
| 10 | 0.033 751 2 | 0.032 730 8 | 1.020 | | −2.6090 | | −38.1 | | | | | | 0.28 |
| 11 | 0.018 685 1 | 0.017 927 | 0.758 | | −2.7426 | | −74.8 | | | | | | 0.25 |
| 12 | 0.010 396 2 | 0.009 851 7 | 0.544 | | −2.8487 | | −142 | | | | | | 0.23 |

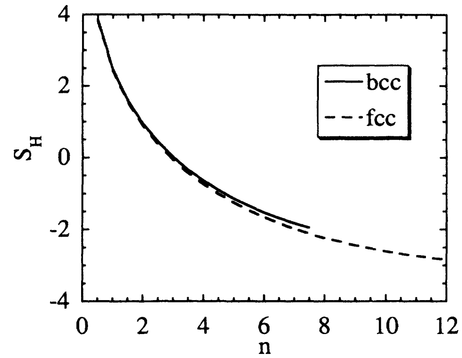


FIG. 2. Harmonic entropy constants $S_{H\mathrm{bcc}}$ and $S_{H\mathrm{fcc}}$ for bcc and fcc lattices, respectively. These constants were evaluated at values of $n$ given by $n=0.5m$, with $m$ a positive integer. The curves are an interpolation.

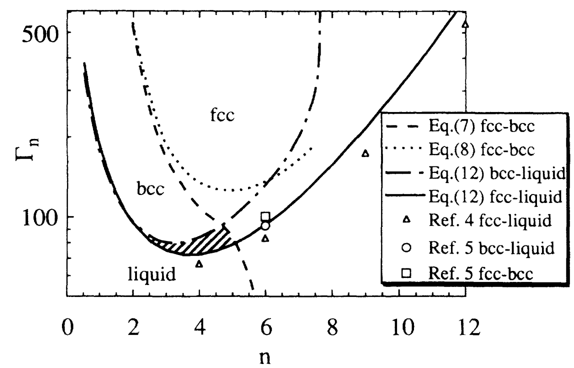


FIG. 4. Phase-equilibrium curves in the $\Gamma_n$ vs $n$ plane. The fcc-bcc curve based on Eq. (7) is dashed; the fcc-bcc curve based on Eq. (8) is dotted. The liquid-solid curves based on the harmonic Lindemann criterion, Eq. (12), are dot-dashed and solid for the bcc-liquid and fcc-liquid transitions, respectively. The fcc-liquid Monte Carlo data of Ref. 4 are shown as triangles; the bcc-liquid and bcc-fcc data of Ref. 5 are the circle and square, respectively. The crosshatched region is thermodynamically inconsistent (see text).

must be applied for $n \leq 3$ in order to hold the lattice together and the lattice is, therefore, incompressible for $n \leq 3$. However, note that $\Delta M \equiv M_{\mathrm{bcc}} - M_{\mathrm{fcc}}$ varies smoothly through the transition from an incompressible to a compressible lattice at $n=3$ [see Fig. 1(b)]. The entropy constants $S_{H\mathrm{bcc}}$ and $S_{H\mathrm{fcc}}$ are also smooth functions through this transition (Fig. 2). However, when $n \rightarrow 7.66$, the bcc lattice becomes unstable and $A_{1\mathrm{bcc}} \rightarrow -\infty$ (see Fig. 3). That is, near instability, long-wavelength finite-amplitude shearing fluctuations reduce the finite-temperature thermodynamic stability of the bcc lattice. However, these shearing fluctuations do not affect the entropy constant $S_{H\mathrm{bcc}}$ since the logarithmic divergence in Eq. (4) is insufficiently singular to cause the sum to diverge as $n \rightarrow 7.66$ (see Fig. 2).

The effect of the first-order anharmonic correction on the polymorphic transition can now be determined by comparing Helmholtz free energies via Eq. (2). Dropping the higher-order anharmonic terms, the difference between the bcc and fcc free energies is

$$\frac{\Delta F_e}{NkT} = \frac{F_{\mathrm{bcc}} - F_{\mathrm{fcc}}}{NkT} = \frac{\Delta M}{2}\Gamma_n - \Delta S_H - \frac{\Delta A_1}{\Gamma_n} . \tag{6}$$

Setting $\Delta F_e = 0$ implies a transition occurs at

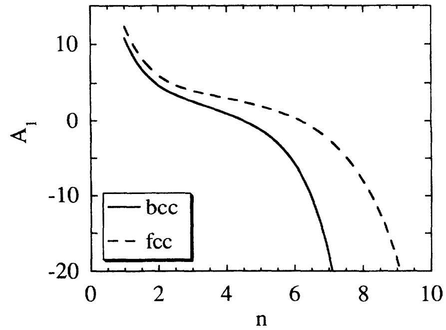


FIG. 3. First-order anharmonic constants $A_{1\mathrm{bcc}}$ and $A_{1\mathrm{fcc}}$ for bcc and fcc lattices, respectively. These constants were evaluated at integer values of $n$ given in Table I. The curves are an interpolation.

$$\Gamma_{\mathrm{fcc-bcc}} = \frac{\Delta S_H \pm \sqrt{\Delta S_H^2 + 2\Delta M \Delta A_1}}{\Delta M} . \tag{7}$$

The results of Hoover *et al.*[3] for this transition are recovered by ignoring the anharmonic term:

$$\Gamma_{\mathrm{fcc-bcc}}^{\mathrm{Harm.}} = 2\frac{\Delta S_H}{\Delta M} . \tag{8}$$

Only the positive root of Eq. (7) provides a physically relevant root which matches onto Eq. (8) in the small $\Delta A_1$ limit. Both of these transition values are tabulated in Table I, and are plotted in Fig. 4.

The effect of the anharmonic term on the fcc-bcc transition is to lower the value of $\Gamma_n$ at the transition relative to the harmonic estimate of Eq. (8)–that is, the region of stability of the bcc phase is reduced. This coincides with the intuitive notion that the existence of an instability in the lattice reduces the number of states available for the lattice vibrations, i.e., soft modes are unbound if they exceed a certain vibrational amplitude which decreases toward zero as instability is approached, so the entropy of the lattice is reduced. Evidently, by keeping the first-order finite-amplitude correction to the free energy we retain this effect, which is naturally neglected in the harmonic approximation. Our result is also in qualitative agreement with the results of Laird and Haymet,[5] who through Monte Carlo calculations also found that for $n=6$, the region over which the bcc lattice is stable is reduced compared to Eq. (8). However, Eq. (7) predicts no stable bcc region for $n=6$, whereas Ref. 5 predicts a very small bcc region. Presumably this discrepancy follows from the neglect of higher-order anharmonic corrections in Eq. (7) which become important near the melting transition.

The use of Helmholtz free energies in the analysis leading to Eq. (7) is rigorously correct only in the incompressible region $n \leq 3$. For $n > 3$, a comparison of Gibbs free energies is appropriate, leading to a slight volume change at transition. The volume change $\Delta V$ is approximately

$$\frac{\Delta V}{V}(\Gamma_n) = \frac{p_{\rm fcc} - p_{\rm bcc}}{X^{-1}} , \tag{9}$$

where the pressure $p$ for each phase is given by

$$\frac{pV}{NkT} = 1 + \frac{n}{3}\frac{E_e}{NkT} , \tag{10}$$

where $E_e/NkT = \Gamma_n d(F_e/NkT)/d\Gamma_n$ is the excess internal energy, and $X^{-1}$ is the inverse isothermal compressibility:

$$\frac{X^{-1}V}{NkT} = 1 + \frac{n}{3}\left[E_e + \frac{n}{3}\Gamma_n \frac{\partial}{\partial \Gamma_n}\frac{E_e}{NkT}\right] . \tag{11}$$

Using Eq. (2) and keeping terms up to $A_1$, the volume change at the transition may be found for $n > 3$ via Eqs. (9)–(11). The compressibility $X$ is dominated by the Madelung energy, which is nearly identical for both lattices, so either $X_{\rm fcc}$ or $X_{\rm bcc}$ may be used in Eq. (9). Results for $\Delta V/V$, keeping the anharmonic correction $A_1$, are tabulated in Table I. This small volume change leads to an inaccessible region in the $\Gamma_n$-$n$ diagram shown in Fig. 4. However, since $\Delta V/V$ is very small, this inaccessible region cannot be seen on the scale of this diagram, and Eq. (7) is an excellent first approximation for the location of the fcc-bcc transition.

The entropy change $\Delta S$ at the transition for $n > 3$ also follows from Eq. (9) if we apply the Clausius-Clapeyron equation $dp/dT = \Delta S/\Delta V$,[9] since the left-hand side of this equation can be evaluated using Eq. (10). Alternatively, one can employ the general relation $\Delta S/Nk \equiv (\Delta E_e - \Delta F_e - \Delta F_{\rm ideal})/NkT$ together with Eq. (2) to obtain

$$\frac{\Delta S}{Nk} \simeq \left[\frac{n}{2}+1\right]\frac{\Delta V}{V} + \Delta S_H + \frac{2\Delta A_1}{\Gamma_{\rm fcc-bcc}} + O\left[\frac{1}{\Gamma_n^2}\right] .$$

Values of $\Delta S$ at the fcc-bcc transition, keeping the first-order anharmonic correction, are tabulated in Table I.

Figure 4 also includes estimates of fcc-liquid and bcc-liquid transitions in order to provide an overall picture of the inverse-power-potential phase diagram. The small volume changes which are predicted to occur for $n > 3$ are neglected. The Monte Carlo data of Hoover, Gray, and Johnson and Laird and Haymet[5] are included, together with data based on the harmonic Lindemann melting criterion,

$$\Gamma_n^{\rm melt} = \frac{\langle \delta x^2 \rangle}{L^2 a^2} = \left[\frac{4\pi}{3}\right]^{(n-1)/3} \frac{\langle \omega_p^2/\omega^2 \rangle}{L^2} , \tag{12}$$

where $\langle \omega_p^2/\omega^2 \rangle \equiv (3N)^{-1} \sum_i \omega_p^2/\omega_i^2$.

The Lindemann parameter $L$ is chosen to be constant as a function of $n$, and its value is chosen separately for the fcc and bcc lattices in order to match the known results for fcc and bcc melting at $n=1$.[7] For the bcc lattice, $L=0.27$ and for the fcc lattice, $L=0.26$. It should be noted that our Lindemann parameter is defined in terms of the Wigner-Seitz radius $a$ rather than the nearest-neighbor spacing since the latter distance is different for different lattices. Values of the lattice sum are given in Table I for fcc and bcc lattices at different values of $n$. Although our values for $\langle \omega_p^2/\omega^2 \rangle$ agree well with those of Ref. 3 at $n=4$, our bcc value at $n=6$ is roughly 4% smaller than that of Ref. 3. We believe this discrepancy stems from the higher numerical accuracy of our results; Ref. 3 used a maximum of $N=8192$ terms in the sum in order to extrapolate to the infinite limit, whereas we employ an efficient technique[10] to effectively keep over $10^6$ terms in the sums for both $S_H$ and $\langle \omega_p^2/\omega^2 \rangle$ before extrapolating to $N=\infty$.

Figure 4 indicates that the Lindemann criterion for the fcc-liquid transition (the solid curve) compares reasonably well to the Monte Carlo results of Ref. 4 (the triangles)—this was pointed out in Ref. 4. However, the Lindemann criterion for the bcc-liquid transition (the dot-dashed line) does not match the Monte Carlo data known for $n=6$ (the circle).[5] Either the harmonic value of $\langle \delta x^2 \rangle$ used in Eq. (12) overestimates the actual bcc position fluctuation near the instability at $n=7.66$, or the Lindemann parameter $L$ has changed significantly from the $n=1$ value. On the other hand, the bcc-liquid curve *should* approach large $\Gamma_n$ as $n \rightarrow 7.66$ since the nearly unstable lattice should melt easily, so the qualitative behavior of the dot-dashed curve must be correct. This implies that the bcc-liquid and fcc-liquid curves must cross (as shown in Fig. 4 at $n \simeq 2$, $\Gamma_n \simeq 100$) since the bcc-liquid transition occurs at a lower $\Gamma_n$ than the fcc-liquid transition for $n=1$.

However, the curves as drawn in Fig. 4 are not thermodynamically consistent in the crosshatched region. In this region the fcc-liquid and bcc-liquid curves imply $F_{\rm bcc} > F_{\rm liquid} > F_{\rm fcc}$, whereas the fcc-bcc curve implies that $F_{\rm fcc} > F_{\rm bcc}$, a contradiction. This paradox is due to the approximate natures of the phase-equilibrium curves. The resolution provides us with useful new information: the three phase-equilibrium curves must cross at a single point. This is analogous to the familiar triple point which occurs in the $p$-$T$ plane at the intersection of three

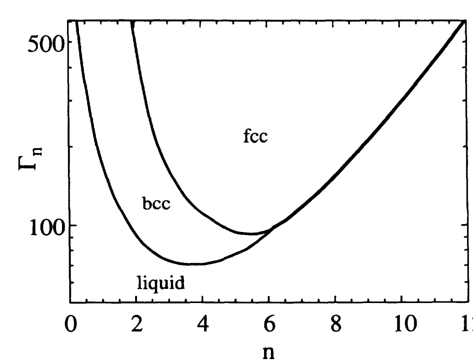


FIG. 5. Best estimate for the phase diagram for the inverse power potentials in the $\Gamma_n$ vs $n$ plane, using the data in Fig. 4.

**free energy surfaces. While it is well known that for inverse-power potentials, there is no such intersection of the free-energy surfaces in the $p$-$T$ plane, apparently an** intersection does occur in the $\Gamma_n$-$n$ plane, so we refer to this intersection as a $\Gamma_n$-$n$ triple point.

The approximate location of the $\Gamma_n$-$n$ triple point may be inferred from our approximate phase-equilibrium curves. The fcc-liquid curve is reasonably well known, and Fig. 4 indicates that the fcc-bcc equilibrium curve crosses the fcc-liquid curve at $n \simeq 5$; the $n = 6$ datum of Ref. 5 argues for a slight shift of the crossing to around $n = 6$. On the other hand, in Fig. 4 the two melting curves appear to cross at $n \simeq 2$, $\Gamma_n \simeq 100$; but this is based on the quantitatively suspect bcc-liquid equilibrium curve. We, therefore, assume that it is this melting curve which is incorrect and draw the $\Gamma_n$-$n$ triple point at $n \simeq 6$. Thus, the inverse-power-potential phase diagram should be close to Fig. 5, which displays our best estimate for this phase diagram based on the data summarized in Table I and Fig. 4. Of course, there could theoretically be several $\Gamma_n$-$n$ triple points separating small regions of bcc stability, but in Fig. 5 we display only the simplest possibility of a single $\Gamma_n$-$n$ triple point. Other less symmetric crystal phases such as hexagonal-close-packed could conceivably also make an appearance (although this seems unlikely). The most important difference between Figs. 4 and 5 is the shift of the bcc-liquid equilibrium curve from the Lindemann result. In order to test this estimate for the bcc melting curve, more accurate Monte Carlo data for the bcc free energy is required for $1 < n < 6$.

This work was supported by NSF Grant No. PHY 91-20240 and ONR Grant No. N00014-89-J-1714, as well as a grant of supercomputer time from the San Diego Supercomputer Center Allocation Committee. The work of H.E.D was performed under the auspices of the U.S. Department of Energy by the Lawrence Livermore National Laboratory under Contract No. W-7405-ENG-48. Useful conversations with W. G. Hoover, D. A. Young, and N. A. Ashcroft are gratefully acknowledged.

[1]D. A. Young, *Phase Diagrams of the Elements* (University of California Press, Berkeley, 1991).

[2]M. Ross, D. A. Young, and R. Grover, J. Geophys. Res. **95**, 21 713 (1990).

[3]W. G. Hoover, D. A. Young, and R. Grover, J. Chem. Phys. **56**, 2207 (1972).

[4]W. G. Hoover, S. G. Gray, and K. W. Johnson, J. Chem. Phys. **55**, 1128 (1971).

[5]B. B. Laird and A. D.-J. Haymet, Mol. Phys. **75**, 71 (1992).

[6]L. Landau and E. Lifshitz, *Statistical Physics, Part 1* (Pergamon, Oxford, 1980), p. 95.

[7]D. H. E. Dubin, Phys. Rev. A **42**, 4972 (1990).

[8]H. Nagara, Y. Nagata, and T. Nakamura, Phys. Rev. A **36**, 1859 (1987).

[9]J. D. Weeks, Phys. Rev. B **24**, 1530 (1981).

[10]D. C. Wallace, *Thermodynamics of Crystals* (Wiley, New York, 1982), pp. 447–462.